VOL. 13, NO. 4, FEBRUARY 2018 ISSN 1819-6608
ARPN Journal of Engineering and Applied Sciences

www.arpnjournals.com

HYDROTHERMAL ALTERATION MAPPING OF MINERALOGICAL IMPRINTS ASSOCIATED WITH SUBTLE GEOTHERMAL SYSTEM USING MIXTURE TUNED MATCHED FILTERING APPROACH ON ASTER VNIR AND SWIR DATA

Aliyu Ja'afar Abubakar[1, 3], Mazlan Hashim[1] and Amin Beiranvand Pour[1, 2]
[1]Geoscience and Digital Earth Centre, Research Institute for Sustainability and Environment, Universiti Teknologi Malaysia, Malaysia
[2]Korea Polar Research Institute, Songdomirae-ro, Yeonsu-gu, Incheon, Republic of Korea
[3]Department of Geography, Faculty of Science, Kaduna State University, P. M. B., Kaduna, Nigeria
E-Mail: mazlanhashim@utm.my

ABSTRACT

The purpose of this study is to evaluate the applicability of Advanced Spaceborne Thermal Emission and Reflection Radiometer (ASTER) Visible near infrared (VNIR) and Shortwave infrared (SWIR) bands in discriminating hydrothermal alteration mineralogy related to thermal springs as proxy for identifying subtle Geothermal (GT) systems at Yankari Park in north eastern Nigeria. The area is characterized by a number of thermal springs including, Gwana, Dimmil, Mawulgo and Wikki which is used directly for recreation and tourism. A Decorrelation Stretch (DCS) transform was initially used on ASTER to highlight alteration zones and generate regions of interest (ROIs) which guided field validation and identification of associated exposed alteration zones. GPS field survey and sampling of hydrothermally altered rocks and laboratory analysis using Analytical Spectral Device (ASD) and X-Ray Diffraction (XRD) is conducted for verification. Observed and validated alteration sites (ROIs) are subsequently used to extract mean image spectra from the ASTER data. We then explored the utility of mean image spectra for mapping subtle mineralogical imprints associated to geothermal systems as proxy for identifying targets in unexplored regions by using the Mixture Tuned Match Filtering (MTMF) algorithm on ASTER VNIR to SWIR spectral subsets. The results indicate that ASTER data could reliably be used for prefeasibility stage narrowing of targets and mapping of subtle alterations using image derived spectra. These could have significant implications especially for mapping unconventional GT systems in unexplored regions.

Keywords: geothermal, hydrothermal alteration, minerals, ASTER, MTMF.

INTRODUCTION

Geothermal (GT) energy is derived from the heat generated by Earth's formation, and subsequent radioactive decay of the earth's minerals [1]. This heat is driven from the core to surrounding rocks which superheats ground water, pressurizing it to the surface. Previously, the exploitive use of geothermal energy was restricted to regions with surface manifestations suggesting the presence of a shallow local heat source, such as hot springs and volcanoes [1]. However, recent technological advancement has dramatically expanded the applicability of this technology [2]. Identifying new GT prospects or monitoring and expanding existing systems using conventional methods is prohibitively costly, time consuming and risky which deter substantial investments in GT exploitation [3].

The capability of remote sensing sensors aboard spaceborne platforms to synoptically identify spatial patterns of hydrothermal alteration mineralogy cost-effectively makes it an attractive means for prefeasibility stage mapping of geothermal systems by proxy for exploration, monitoring and narrowing of prospective sites [4, 5]. Hydrothermal alteration minerals such as clays, sulfates, carbonates, silicates and iron oxides exhibit diagnostic spectral reflectance characteristics that allow for their remote detection. This is made possible using the Visible near infrared (VNIR), Shortwave infrared (SWIR) and Thermal infrared (TIR) regions of the Electromagnetic spectrum (EMS), which has been shown to be reliably suited for discrimination and recognition of these mineral assemblages [6]. In particularly, the SWIR radiation is the best spectral region of the EMS for sensing various aspects of hydrothermal alteration zones [7]. Hydroxyl-bearing (OH) minerals including clay and sulfate groups as well as carbonate minerals present diagnostic spectral absorption features due to vibrational processes of fundamental absorptions of Al–O–H, Mg–O–H, Si–O–H, and CO3 groups in the shortwave infrared radiation region [8]. Consequently, this wavelength region provides the best means to explore and map hydrothermal alteration zones associated with GT systems. The most important characteristics of the SWIR wavelength region is the possibility of identifying and mapping the spatial distribution of hydrothermal alteration minerals containing OH groups [9].These minerals are by products of metasomatism in hydrothermal systems and serve as important geothermometer for mapping GT sites [10]. The ASTER data is especially suited for mapping these unique alteration minerals due to its improved spectral bands in the VNIR (0.52-0.86um) and 6 bands in the SWIR (1.6-2.43um) having 15m and 30m spatial resolution respectively [11]. The iron oxides minerals and vegetation are thus mapped in the VNIR region, while the SWIR is designed for mapping surface soil and especially hydrothermal alteration minerals [12]

Many previous studies have demonstrated the significance of mapping hydrothermal alteration and indicator minerals for identifying GT systems using

remote sensing [4, 5, 13, 14]. However, these studies have not adequately examined the utility of mean image spectra in peculiar and unconventional GT settings with characteristically subtle surface manifestations and particularly by exploring the use of sub-pixel fractional abundance estimation using field verified image derived spectra as reference. Surely, an inclusion of a field certified image spectra will increase the reliability of image analysis results especially in such areas with limited primary data.

In this study, we demonstrate the utility of image spectra extracted from regions of interest (ROIs) which have been validated in the field using comprehensive GPS rock sampling survey of unique alterations of interest and laboratory Analytical Spectral Device (ASD) and X-Ray Diffraction analysis. The study essentially evaluated ASTER (VNIR-SWIR) data for mapping hydrothermal alteration zones related to GT systems (thermal springs) by employing the Mixture Tuned Matched Filtering (MTMF) algorithm for partial sub-pixel spectral mapping of specific indicator minerals as targets, in an unexplored area of Yankari Park in NE Nigeria. The area is characterized by several thermal springs including Wikki, Mawulgo, Dimmil and Gwana.

The peculiarities of the terrain as compared to other well investigated regions using remote sensing techniques such as the extensional areas of the USA [4] , volcano-tectonic regions in Asia [15] and others, provides a unique setting for testing the sensors and methods in mapping subtle GT systems characterized by hydrothermally altered rocks and minerals including ; Clays, Carbonates, Sulfates and Silicates which are GT indicators difficult to discern using only conventional techniques [13].

STUDY AREA GEOLOGY

The Yankari Park is located within Latitude 9.7500^0N, and Longitude 10. 5000^0E in Bauchi State, northeastern Nigeria. Territorially it extends to about 2,244 square kilometers (866 sq. mi). Thermal springs in the Park include; Dimmil, Gwana and Mawulgo. The famous Wikki thermal spring which has a temperature of about 37^0 C degrees Celsius has been used for recreation and as a tourist attraction in the Park. Geologically, Yankari Park is within the Kerri formation characterized by Neogene to Mesozoic older sedimentary rocks which is composed of sandstone, silt stones, kaolinites, grits and clays [16]. Yankari is also part of the Benue Trough, bordered to the west by the basement complex crystalline rocks of the Jos plateau, to the northeast by the Biu plateau and to the southeast by the Adamawa highlands. The Nigerian land mass is an aseismic intra-plate, tectonically stable, however, historical data indicate minor crustal disturbances have occurred in the last 50 years in different locations in the country [16]. There are many extinct volcanic features in the Jos plateau and the north eastern and western part of the country. In 2011, a fumarole activity were observed at Abaduguri range in Funakaye area northeast of the Yankari Park which is believed to have magmatic origins [16]. Figure-1 illustrates Nigeria's geological areas with location of Yankari Park. Figure-2 shows the map of Yankari Park and areas where field work and image analysis are conducted.

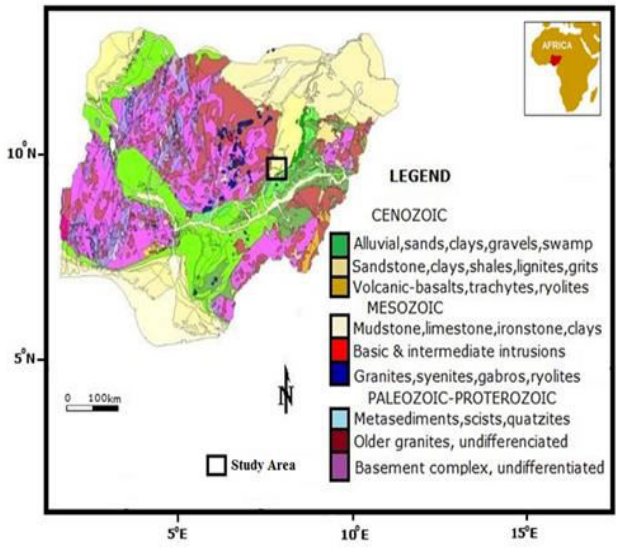

Figure-1. Geological map of Nigeria showing Yankari park study area location (modified from [16]).

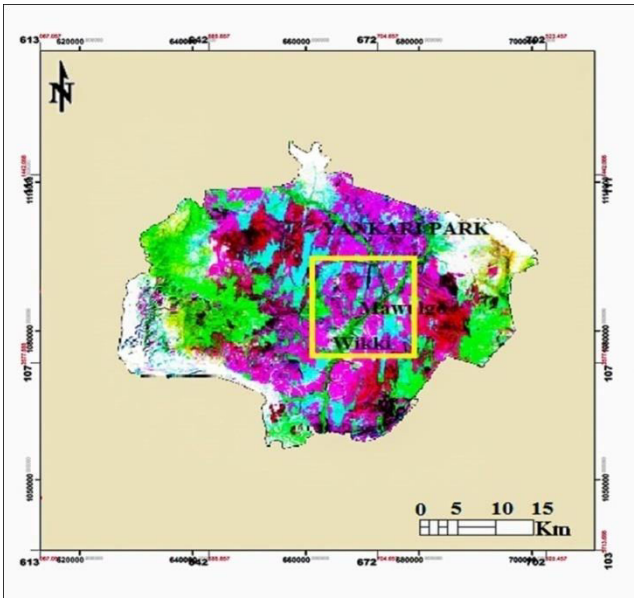

Figure-2. Map of Yankari park showing areas where field work and image analysis was focused.

MATERIALS AND METHODS

Aster data pre-processing

A cloud free ASTER L1T scene (AST_L1T_00301252006095330 path/raw, 187/53) covering part of the Yankari Park with acquisition date of 25th, January 2006 obtained from U.S. Geological EROS (http://glovis.usgs.gov/) is used for this study. The ASTER level 1T is a Precision Terrain Corrected Registered At-Sensor Radiance that has been geometrically rectified, and turned to a north-up Universal Transverse Mercator

(UTM) 32N projection with WGS 84 Datum [11]. The crosstalk correction was applied to the SWIR subsystem to rectify the ghost effect caused by detector energy leakage from band 4 which spills into bands 5 and 9 [17]. The VNIR and SWIR bands are first layer stacked into a cube and resampled. A spatial subset (of 1515 sample by 1515 lines) is then made covering the Mawulgo and Wikki thermal spring areas visited in the field (Figure-2). A two way Atmospheric correction was done using the Internal Average Relative Reflection-IARR. The IARR involves calculation of the average scene spectrum which is used as the reference spectrum; this is then divided into the spectrum at each pixel of the image to generate relative reflectance [18] and the Fast Line-of-site Atmospheric Analysis of Spectral Hypercubes- FLAASH [19]. The FLAASH algorithm derives its first-principles physics-based calculations from the MODTRAN4 radiative transfer code [20]. The FLAASH is mathematically computed as:

$$L = \left(\frac{\mathrm{A}p}{1 - p_e S} \right) + \left(\frac{\mathrm{B}p_e}{1 - p_e S} \right) + L_a \quad (1)$$

Where:

ρ is the pixel surface reflectance

ρ_e is an average surface reflectance for the pixel and a surrounding region

S is the spherical albedo of the atmosphere

L_a is the radiance back scattered by the atmosphere

A and B are coefficients that depend on atmospheric and geometric conditions but not on the surface

The ENVI 5.1 preprocessing calibration utilities was used for both corrections. The image is converted from radiance to reflectance to facilitate subsequent spectral analysis [21]. The summary of data characteristics of ASTER is shown in Table-1.

Table-1. ASTER sensor characteristics [22].

Instrument	ASTER
Spectral range	0.5-0.9 (VNIR) 1.6-2.4 (SWIR) 8.1-11.7 (TIR) (in microns)
Visible near infrared bands	4
Shortwave infrared bands	6
Thermal bands	5
Spatial resolution	15, 30, 60 m
Temporal resolution	16 days
Swath width	60 km

Image processing methods

Decorrelation stretch (DCS)

An initial DCS transform was used to highlight alteration areas of interest using the resampled ASTER VNIR-SWIR bands with specific alteration mineral features in mind. DCS is an image enhancement technique which is capable of highlighting out subtle image elements that are nearly invisible in true colour composites by reducing inter-band correlations and improving the visualization of features such as possible hydrothermal alteration zones [7]. An ASTER DCS have been shown to be useful in an initial GT mapping at regional scale as it highlights unique alteration minerals such as clays, sulfates and calcites [13] which are useful indicators of GT activity, especially if verified by a field survey. It is employed in this study to visually heighten the spectral variations among 3 input bands. The bands are selected based on specific diagnostic absorption features of the targeted alterations of interest specifically; Argillic, Calcite and Iron oxide/hydroxide related alterations using ASTER bands 6, 8 and 3. Clays e.g. kaolinite-dickite-illite have diagnostic absorption features around 2.20um (equivalent to ASTER band 6), Calcites at 2.33um (bands 8) in the SWIR region [8]. Iron oxides e.g. Hematite and Limonite have diagnostic features around 0.48um and 0.83-0.97um [8] in the VNIR (ASTER bands 2 & 3). Observations are described in results and discussions. A summary of the study methods is shown in Figure-3.

Extraction of mean image spectra

Diagnostic spectral characteristics of alteration minerals of interest were used as guide to extract mean image spectra as reference from identified alterations verified in the field during GPS field survey. An exposed alteration area around Mawulgo thermal spring designated Mawulgo 2 (M2) (see Figure-5) is used for analysis. The hydrothermally altered rocks from the region are also sampled and used for XRD laboratory analysis. Observed alteration area coordinates are used to trace points as regions of interest (ROIs) on the image and extraction of image spectra is done using the Z-profile and pixel locator methods [23]. Alterations observed in the studied area are predominantly argillic, calcite and limonitic, accordingly, clays, carbonates and iron oxides minerals such as Kaolinite, calcites and hematite, are specifically extracted as end members and the mean spectra are compared with corresponding ASTER USGS spectral library by considering the shape and position of diagnostic absorption features of the minerals to substantiate results as shown in Figures 4 (a) and (b). The extracted mean spectra are subsequently used as end member reference to classify the image and identify surface compositional features of pixels in the M2 region as targets using the MTMF algorithm [24].

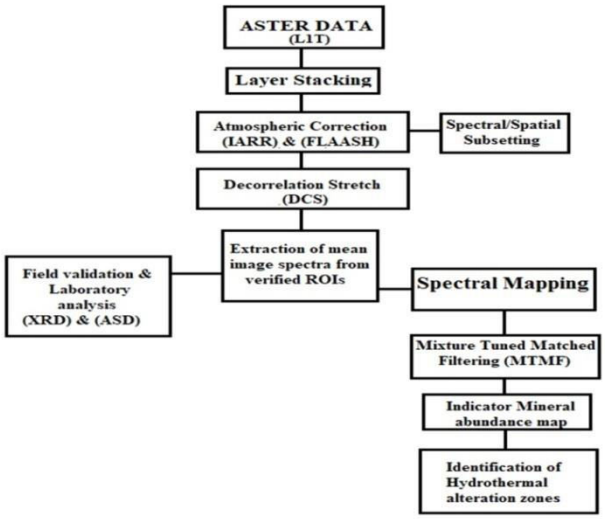

Figure-3. Simplified flow chart of the study methods.

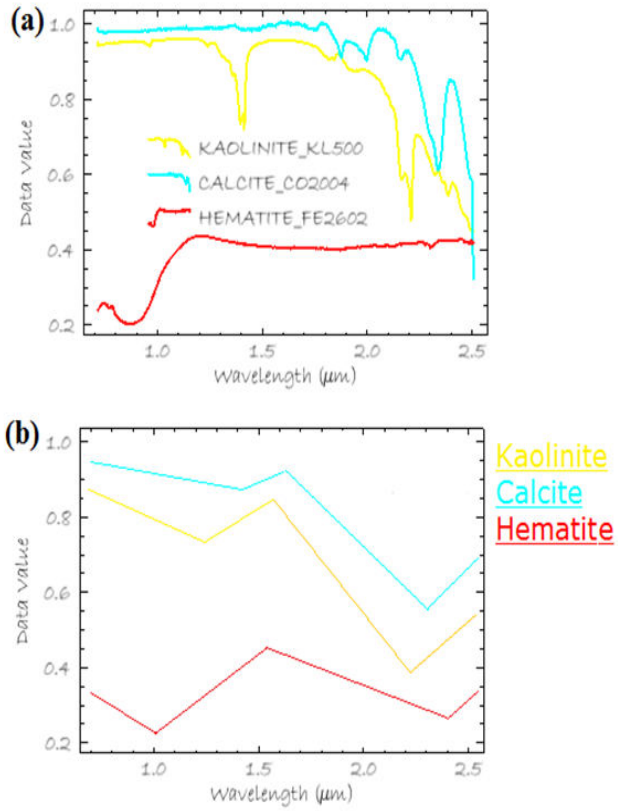

Figure-4. (a) ASTER USGS library spectra for the 3 end members used to compare and extract mean image spectra for corresponding end members (b) Mean image spectra of end members extracted from ASTER image data at verified ROIs.

Mixture tuned matched filtering (MTMF) method

In this study The MTMF [25] is used. It is a partial unmixing algorithm suitable for analysis especially when the study objective is to identify fewer targets from unwanted background data. It is a data driven method which is a hybridization of the Matched Filtering (MF) [26] and the Linear Spectral Unmixing (LSU) [27]. It combines the strengths of the MF in that it has no requirement for knowledge of all the endmembers while avoiding the constraints of the LSU in which the spectral signature at any given pixel is a linear combination of the individual components contained in that pixel [25]. The MTMF is composed of two components, the Matched Filtering (MF) and the Mixture Tuned (MT) stage. The latter identifies and rejects false positives while the former estimates sub pixel endmember abundances. To implement the MTMF, a spatial and spectral subset of the ASTER data was made containing only the stacked VNIR-SWIR bands and covering only the field surveyed areas of Yankari Park. This was imported into ENVI 5.1 and the Spectral Hourglass approach used for systematic analysis starting from Minimum Noise Fraction (MNF), n-D visualization, Pixel Purity Index (PPI), User supplied extracted endmember spectra and MTMF analysis. The results of the MTMF on ASTER data are illustrated using a combination of gray images loaded as RGB indicating sub-pixel abundances of each endmember in assigned colours and using 2D scatter plots to identify pure pixel abundance as targets as shown in results and discussions in Figures 6, 7 and 8.

Field and laboratory methods

Field survey was conducted from 15-18th August at the study area. GPS mapping and sampling of alteration areas and GT features was guided by the works of Coolbaugh, *et al.* [28] to improve understanding of structural complexities that are not easily comprehensive on the image [28]. Twenty seven (27) Sampled points were identified and marked while 45 rock samples are obtained. M2 ROI around Mawulgo (see Figure-5), an exposed area, is investigated in this study. Acquired altered rocks from the GPS survey were analyzed using the latest smart Lab X-ray Diffractometer technology (Rigaku) at the University Teknologi Malaysia (UTM) UPMU laboratory, which indicated several alteration minerals of GT importance. Spectral reflectance measurements were made using an Analytical Spectral Devices (ASD) Spectroradiometer Fieldspec® model, which records at a spectral range of 325–2500 nm (nanometer) with a 10 nm individual band width. The spectral measurements were performed in the Remote Sensing laboratory at the Universiti Teknologi Malaysia (UTM) using a contact probe and a built-in illumination source.

RESULTS AND DISCUSSIONS

Decorrelation stretch (DCS)

The results of the DCS for bands 6, 8 and 3 is loaded as RGB as shown in Figure-4. Possible argillic alteration appear as pink-purple instead of red signifying weak alteration [13], calcite appear green and iron oxides appear as blue. However, along river Gaji which is vegetated, appear dark blue indicating a poor discrimination between iron oxides and vegetation spectra

by the broad bands of ASTER because both features have strong absorptions in band 3 (0.78-0.83um)[29]. ROIs M2 indicate especially weak alteration signifying the need for further investigation.

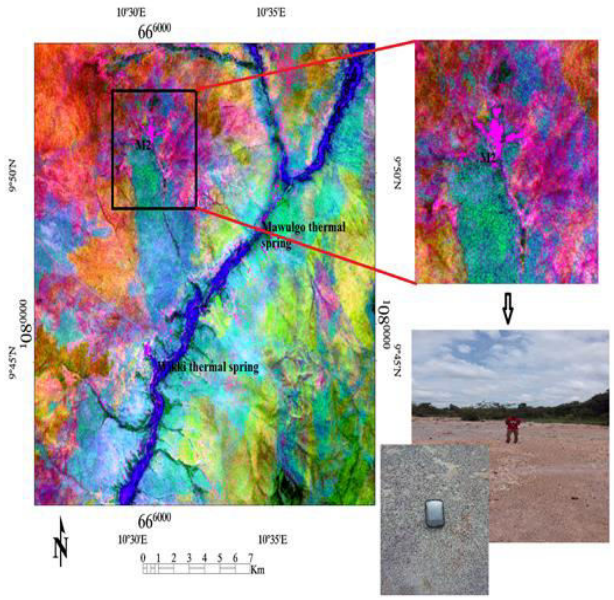

Figure-5. DCS bands 6, 8, and 3 in RGB showing possible argillic, calcite and iron oxide alteration zones.

Mixture tuned matched filtering (MTMF) results

The result of MTMF is presented in figure 6. It revealed predominantly argillic alteration with pixel abundance of kaolinite (yellow) at M2 sometimes encircling calcite alteration (cyan). Possible prospects of similar pattern are observed south western and eastern portions of Mawulgo 2 (M2). The results agrees with observations made in the field as shown in the DCS image and plates in Figure-5. However, iron oxide related alterations appear randomly (red pixels) and could not be suitable for narrowing targets (Figure-6). The occurrence of argillic and calcite alteration centrally at M2 which are exposed areas observed in the field to have hydrothermally altered kaolinite deposits around Mawulgo thermal spring, reliably aid in narrowing targets for in depth investigation especially for similar pixel abundance discriminated within the image. The discrimination of kaolinite and calcite alterations clearly at M2 and at other prospective zones in the image by the MTMF algorithm agrees with observations made in the field of hydrothermally altered rocks. To further ascertain the results and sieve out errors and false alarms, an MF score image is created in Figure-7 and also a 2D scatter plot of MF score versus infeasibility in Figure-8.

The results of MF scores in Figure-7 indicates endmember sub-pixel abundance for kaolinite-calcite-hematite as a-b-c represented by brighter pixels, while pixel abundance for kaolinite Figure-7(a) appear clearly around M2, calcite appear randomly Figure-7(b) and hematite abundance appear haphazardly Figure-7(c). There is however, confusion in the discrimination of the end member indicator minerals in Figure-7 MF results when compared with the MTMF result in Figure-6.

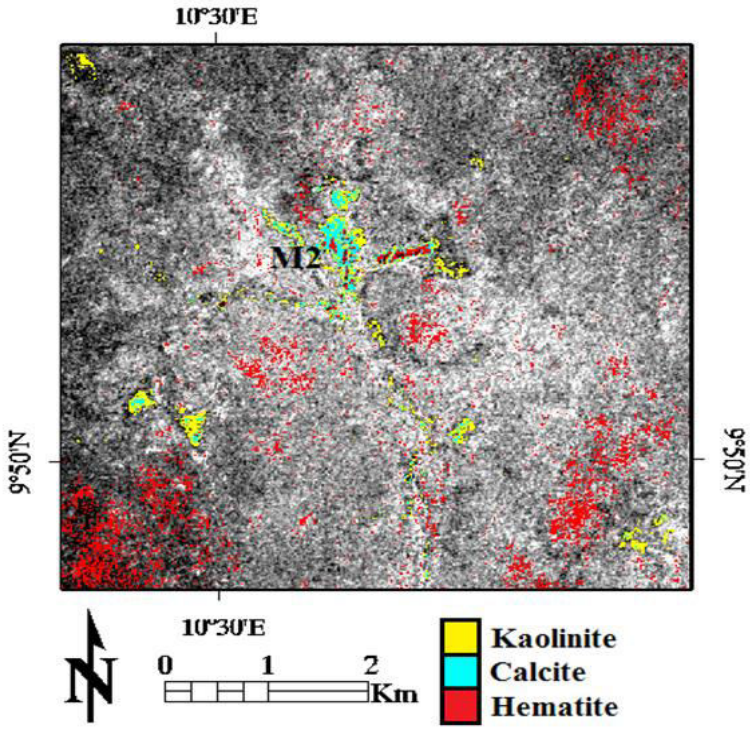

Figure-6. Result of MTMF sub-pixel abundance map for 3 endmembers used as reference.

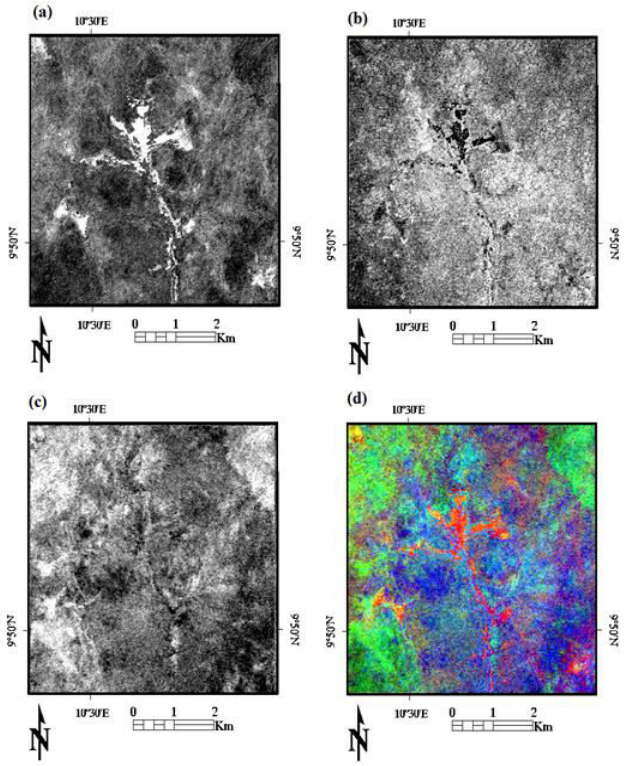

Figure-7. MF score image for (a) kaolinite, (b) calcite, and (c) hematite as gray scale (bright pixels) and (d) as RGB.

The 3 alteration indicators are loaded as RGB in Figure-6(d) for kaolinite-hematite-calcite. It was observed that the result mostly corroborates areas visited in the field and identified as argillic alteration zones with kaolinite deposits at M2. The MF score image however, poorly discriminates the endmembers especially when compared with the MTMF result in Figure-6 due to false positives [24]. A 2D scatter plot is thus made for MF score versus Infeasibility in order to clearly identify the purest pixels which could serve as target to corroborate ground investigation. The results of the scatterplot are presented in Figure-8.

The results of the 2D scatterplot is shown in Figure-8 (a, b, c). It was observed that the 2D scatterplot better identified valid detections of target alteration zones as against the MF score image in figure 6. A criteria was used in which the best pixels are selected using the scatter plot, where the MF score for these pixels corresponds to abundance (a range of 0 - 1.0 which equals percentage abundance between 0 and 100%) [23]. As observed from figure 8 (a), valid detections for kaolinite are found around 0.73 (~73% abundance) close to 1 signifying higher MF score with low infeasibility score at the extreme right of the plot [24] as indicated by yellow pixels (Figure-8a). While Figure-8 (b) for calcites, pixels with high MF score and low infeasibility are detected around 0.55 (~55% abundance) and around 0.63 (~63% abundance) for hematite as shown in figure 8 (c). By exporting the pixels with the high MF scores and correspondingly low infeasibility, the purest pixel abundance of the indicator minerals were identified and depicted as shown on the images beside the scatterplots (Figure-8). In a nut shell, the results show a pure abundance for kaolinite from approximately 70 to 100%, 50 to 100% for calcite and 60 to 100% for hematite. The most pixels in the scatter plots that have high infeasibility and low MF scores are false alarms and represent rejected errors by the MTMF algorithm [24]. This signifies the MTMF as a robust algorithm for target detection especially as most of the valid detection pixels corroborate areas identified and verified in the field particularly for kaolinite and calcite concentrated around M2. Results of iron oxide abundance were rather random and sparse and could not conservatively be used for target detection of alteration related to proximate areas of the GT systems.

Results of field and laboratory assessments

The results of XRD laboratory analysis is employed to substantiate image analysis. It shows the presence of kaolinite and Quartz as dominated alteration minerals in the collected rock samples at Mawulgo 2 (M2) (Figure-9). The occurrence of kaolinite in the M2 sample, which is an important phyllosilicates mineral unique to hydrothermal systems, was a significant indicator of geothermal activity [30]. Kaolinite in the sample also corroborated image analysis results as discriminated by the MTMF algorithm, however, calcite and iron oxide were not identified in the XRD at M2.

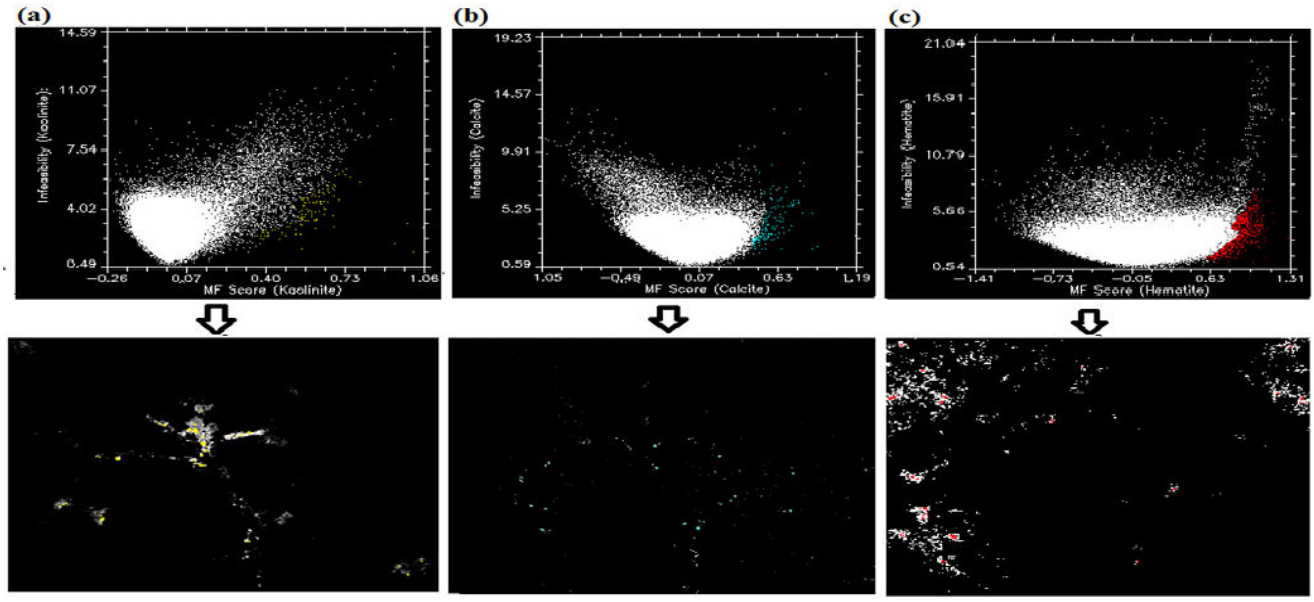

Figure-8. Results of 2D scatterplot of MF score versus Infeasibility for (a) kaolinite (b) calcite and (c) hematite exported to ROI image depicting pure sub-pixel abundance for argillic, calcite and iron oxide alteration zones.

Moreover, Argillic alteration plays a key role in the formation of clay minerals, including kaolinite, smectite and illite, which is generally a low-temperature event [31]. The earliest signs of argillic alteration include the bleaching out of feldspars [31]. Advanced argillic alteration, a subcategory of argillic alteration, consists of kaolinite + quartz + hematite + limonite, feldspars leached and altered to sericite [32]. The presence of this assemblage suggests low pH (highly acidic) conditions and temperatures [32]. The identification of quartz and or silicon dioxide in the M2 samples signifies phyllic alteration [33], a hydrothermal alteration resulting from the circulation of hot fluids or metasomatism aided by the permeability of rocks such as the sedimentary formation [30]. Phyllic alteration is often closely associated with argillic alteration, which occurs at lower temperatures and dominantly affects plagioclase [34]. The occurrence of quartz at M2 (Figure-9) signifies that the study zones may be fossilized geothermal systems. It is characterized by hydrothermal systems especially since silica is known to occur as quartz when aged over time [32]. The result of the spectral measurement using the ASD on the sample from M2 was in agreement with the XRD results and shows strong absorption around 2200 nanometer which is diagnostic of clay minerals [8] indicating argillic alteration. The geological and mineral resource map of Bauchi state from the Nigerian Geological Survey Agency (2006), was also studied and affirmed that the areas where the study is conducted is characterized by sandstones, shale and clay.

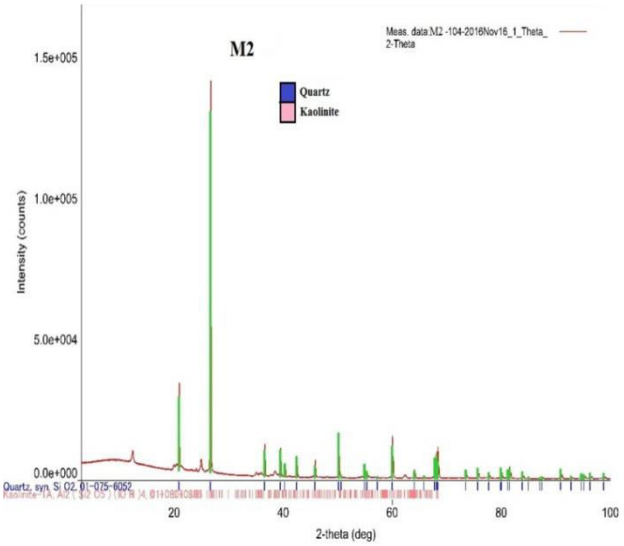

Figure-9. Results of XRD of hydrothermally altered rock samples at Mawulgo 2 (M2).

CONCLUSIONS

In conclusion, the spectral information extraction using the MTMF algorithm reveals that it is a robust technique for mapping surface compositional features of hydrothermal alteration related to proximate GT systems especially where such are exposed widely enough to be detected by the 15m to 30m ASTER VNIR to SWIR channels respectively. The MTMF results indicate pixel abundances which agrees with field and laboratory ASD and XRD validated results. However, while the MF results reveals many pixels abundances as errors, the use of the 2D scatter plot rejects false positives resulting in the discrimination of pure valid detections in conformity with the MTMF results. This signifies the method as a robust and cost effective technique that can be adequately

employed for prefeasibility stage narrowing of alteration zones associated with GT systems to aid further investigation and or identification of prospective GT sites. We discovered that GPS sampling of exposed alterations and subsequent extraction of image spectra using coordinates of verified locations on the image increased the accuracy of spectral mapping of identified alteration zones. Our integration of comprehensive and detailed field validation, the use of image spectra verified using laboratory analysis and the use of multispectral ASTER VNIR-SWIR data could be valuable for GT exploration using indicator minerals in unexplored regions especially where cost-effective exploration strategies are needed.

ACKNOWLEDGEMENT

The authors wish to acknowledge the University of Technology Malaysia, Kaduna State University and Kaduna State Government, Nigeria, for providing the facilities and support for this investigation. We are also thankful to Korea Polar Research Institute (KOPRI) for their assistance in preparation of the manuscript and the Earth Resources Observation System (EROS) Data Centre of the U.S.G.S. from which the image data used for the study was obtained.

REFERENCES

[1] W. E. Glassley. 2014. Geothermal energy: renewable energy and the environment: CRC Press.

[2] P. Olasolo, M. Juárez, M. Morales, and I. Liarte. 2016. Enhanced geothermal systems (EGS): A review. Renewable and Sustainable Energy Reviews. 56: 133-144.

[3] A. Daniilidis and R. Herber. 2017. Salt intrusions providing a new geothermal exploration target for higher energy recovery at shallower depths. Energy. 118: 658-670.

[4] W. M. Calvin, E. F. Littlefield and C. Kratt. 2015. Remote sensing of geothermal-related minerals for resource exploration in Nevada. Geothermics. 53: 517-526, 1.

[5] C. Kratt, W. M. Calvin, and M. F. Coolbaugh. 2010. Mineral mapping in the Pyramid Lake basin: Hydrothermal alteration, chemical precipitates and geothermal energy potential. Remote Sensing of Environment. 114: 2297-2304.

[6] G. R. Hunt and R. P. Ashley. 1979. Spectra of altered rocks in the visible and near infrared. Economic Geology. 74: 1613-1629.

[7] A. B. Pour and M. Hashim. 2015. Hydrothermal alteration mapping from Landsat-8 data, Sar Cheshmeh copper mining district, south-eastern Islamic Republic of Iran. Journal of Taibah University for Science. 9: 155-166.

[8] R. N. Clark. 1999. Spectroscopy of rocks and minerals, and principles of spectroscopy. Manual of remote sensing. 3: 3-58.

[9] J. F. Huntington. 1996. The role of remote sensing in finding hydrothermal mineral deposits on Earth. in Ciba Foundation Symposium. pp. 214-235.

[10] R. W. Renaut, R. B. Owen and J. K. Ego. 2017. Geothermal activity and hydrothermal mineral deposits at southern Lake Bogoria, Kenya rift valley: Impact of lake level changes. Journal of African Earth Sciences, 2017.

[11] M. Abrams. 2000. The Advanced Spaceborne Thermal Emission and Reflection Radiometer (ASTER): data products for the high spatial resolution imager on NASA's Terra platform. International Journal of Remote sensing. 21: 847-859.

[12] Y. Yamaguchi and C. Naito. 2003. Spectral indices for lithologic discrimination and mapping by using the ASTER SWIR bands. International Journal of Remote Sensing. 24: 4311-4323.

[13] E. F. Littlefield and W. M. Calvin. 2014. Geothermal exploration using imaging spectrometer data over Fish Lake Valley, Nevada. Remote Sensing of Environment. 140: 509-518.

[14] K. A. Reath and M. S. Ramsey. 2013. Exploration of geothermal systems using hyperspectral thermal infrared remote sensing. Journal of Volcanology and Geothermal Research. 265: 27-38.

[15] A. Saepuloh, A. Susanto, P. Sumintadireja and E. Suparka. 2015. Characterizing Surface Manifestation of Geothermal System under Torrid Zone using Synthetic Aperture Radar (SAR) Data. in Proceedings of the World Geothermal Congress.

[16] E. Kurowska and S. Krzysztof. 2010. Geothermal exploration in Nigeria. in Proceedings World Geothermal Congress.

[17] H. Tonooka and A. Iwasaki. 2004. Improvement of ASTER/SWIR crosstalk correction. in Remote Sensing. pp. 168-179.

[18] F. Moore, F. Rastmanesh, H. Asadi and S. Modabberi. 2008. Mapping mineralogical alteration using

principal-component analysis and matched filter processing in the Takab area, north-west Iran, from ASTER data. International Journal of Remote Sensing. 29: 2851-2867.

[19] T. Perkins, S. Adler-Golden, M. W. Matthew, A. Berk, L. S. Bernstein, J. Lee, *et al*. 2012. Speed and accuracy improvements in FLAASH atmospheric correction of hyperspectral imagery. Optical Engineering. 51: 111707-1-111707-7.

[20] G. P. Anderson, G. W. Felde, M. L. Hoke, A. J. Ratkowski, T. W. Cooley, J. H. Chetwynd Jr, *et al*. 2002. MODTRAN4-based atmospheric correction algorithm: FLAASH (Fast Line-of-sight Atmospheric Analysis of Spectral Hypercubes). in AeroSense 2002. pp. 65-71.

[21] A. B. Pour and M. Hashim. 2015. Evaluation of Earth Observing-1 (EO1) Data for Lithological and Hydrothermal Alteration Mapping: A Case Study from Urumieh-Dokhtar Volcanic Belt, SE Iran. Journal of the Indian Society of Remote Sensing. 43: 583-597.

[22] NASA. National Aeronautics and Space Administration (NASA). Landsat Science. Landsat.gsfc.nasa.gov [Online].

[23] I. Research Systems. 2008. ENVI Tutorials. Research Systems, Inc., Boulder, CO.

[24] J. W. Boardman and F. A. Kruse. 2011. Analysis of Imaging Spectrometer Data Using $ N $-Dimensional Geometry and a Mixture-Tuned Matched Filtering Approach. IEEE Transactions on Geoscience and Remote Sensing. 49: 4138-4152.

[25] J. W. Boardman and F. A. Kruse. 1994. Automated spectral analysis: a geological example using AVIRIS data, north Grapevine Mountains, Nevada. in Proceedings of the Thematic Conference on Geologic Remote Sensing. pp. I-407.

[26] J. C. Harsanyi and C.-I. Chang. 1994. Hyperspectral image classification and dimensionality reduction: An orthogonal subspace projection approach. IEEE Transactions on geoscience and remote sensing. 32: 779-785.

[27] F. van der Meer. 1996. Spectral mixture modelling and spectral stratigraphy in carbonate lithofacies mapping. ISPRS journal of photogrammetry and remote sensing. 51: 150-162.

[28] M. Coolbaugh, C. Sladek, and C. Kratt. 2004. Digital mapping of structurally controlled geothermal features with GPS units and pocket computers: Proceedings. in Annual Meeting, Palm Springs, CA, Aug. pp. 321-325.

[29] A. B. Pour and M. Hashim. 2015. ASTER, ALI and Hyperion sensors data for lithological mapping and ore minerals exploration. Springer Plus. 3: 1.

[30] H. P. Heasler, C. Jaworowski, and D. Foley. 2009. Geothermal systems and monitoring hydrothermal features. Geological Monitoring. pp. 105-140.

[31] P. Sanchez-Alfaro, M. Reich, G. Arancibia, P. Pérez-Flores, J. Cembrano, T. Driesner, *et al.* 2016. Physical, chemical and mineralogical evolution of the Tolhuaca geothermal system, southern Andes, Chile: Insights into the interplay between hydrothermal alteration and brittle deformation. Journal of Volcanology and Geothermal Research. 324: 88-104.

[32] K. Mauriohooho, S. L. Barker, and A. Rae. 2016. Mapping lithology and hydrothermal alteration in geothermal systems using portable X-ray fluorescence (pXRF): A case study from the Tauhara geothermal system, Taupo Volcanic Zone. Geothermics. 64: 125-134.

[33] M. Todbileg, B. Gorte, F. van Ruitenbeek and B. Maathuis. 2003. Identification of Silicification Using Airborne Thermal Infrared Data in the Panorama, Pilbara, Australia. Ed.

[34] W. Parry, M. Jasumback, and P. N. Wilson. 2002. Clay mineralogy of phyllic and intermediate argillic alteration at Bingham, Utah. Economic Geology. 97: 221-239.